Bull. Disas. Prev. Res. Inst., Kyoto Univ., Vol. 44, Part 1, No. 379, March, 1994

Estimation of Strong Ground Motions on Hard Rock and Soft Sediment Sites in the Ashigara Valley Using the Empirical Green's Function Method

By Jorge AGUIRRE, Kojiro IRIKURA and Kazuyoshi KUDO*

(*Manuscript received on June 16, 1993, revised on March 18, 1994*)

Abstract

We applied the Empirical Green's Function Method to simulate ground motions on hard rock and soft sediment at near distance (8 km) for the 1990 Hakone earthquake ($M_{JMA}=5.1$) using the records of the foreshock ($M_{JMA}=2.9$). We examined the seismic data used in the Ashigara Valley Blind Prediction Test (Kudo, 1992), records from weak and strong motions observed at 3 superficial and 2 borehole sites. The main goal of this study is to investigate the non-linear behavior of soft soil at KS1 and KS2 sites. Our method is based in a linear superposition of ground motions, which allows us to check the non-linear effect in soft sediments due to strong motions (more than 100 gals) by comparing the observed waveforms with the simulated ones. The simulation method proposed by Irikura (1986) is modified in order to correct a difference in stress drop that was found between these two events. We found the stress parameters play an important role in the simulations. The seismic source model is determined by using only rock sites waveforms, which is effected by minimizing the residuals between the synthetics and the observed waveforms. First we used a long time window to obtain the source model. Second, a time window of 3 seconds including the onsets and largest amplitudes of the S-wave part was used to determine the source model, avoiding contamination by seismic noises in the small event records. After defining the seismic source model we simulated the ground motions at KD1, KS1 and KS2, and compared the simulated with the observed seismograms. We found, the difference between the acceleration waveforms (synthetic and observed) to be relatively large at KS1 and KS2 compared to the rest of the sites, and we conclude that a non-linear effect during the 1990 Hakone earthquake ($M_{JMA}=5.1$) at KS2 and KS1 exists, based on these. From the comparison of their spectra, we could not find systematic changes of the predominant frequencies between the observed and synthetic at KS1 and KS2.

Introduction

The importance of site effects is well known for predicting ground motions from engineering interest and for understanding crustal structures and source processes from seismological interest. Recently two international test fields have been made with the purpose of evaluating the state-of-the-art on-site-effect simulations. One of them is the Ashigara Valley Blind Prediction Test. For that experiment, two events were selected, mainshock ($M_{JMA}=5.1$) and foreshock ($M_{JMA}=2.9$), and five stations were chosen. One is located on rock outcrop (KR1), two on soft sediments (KS1 and KS2), and two in borehole, under KS2, at a depth of 30 (KD 1) and 97 (KD2) meters from the surface (**Figure 1**). The goal in that experiment was to

* Earthquake Research Institute, University of Tokyo.

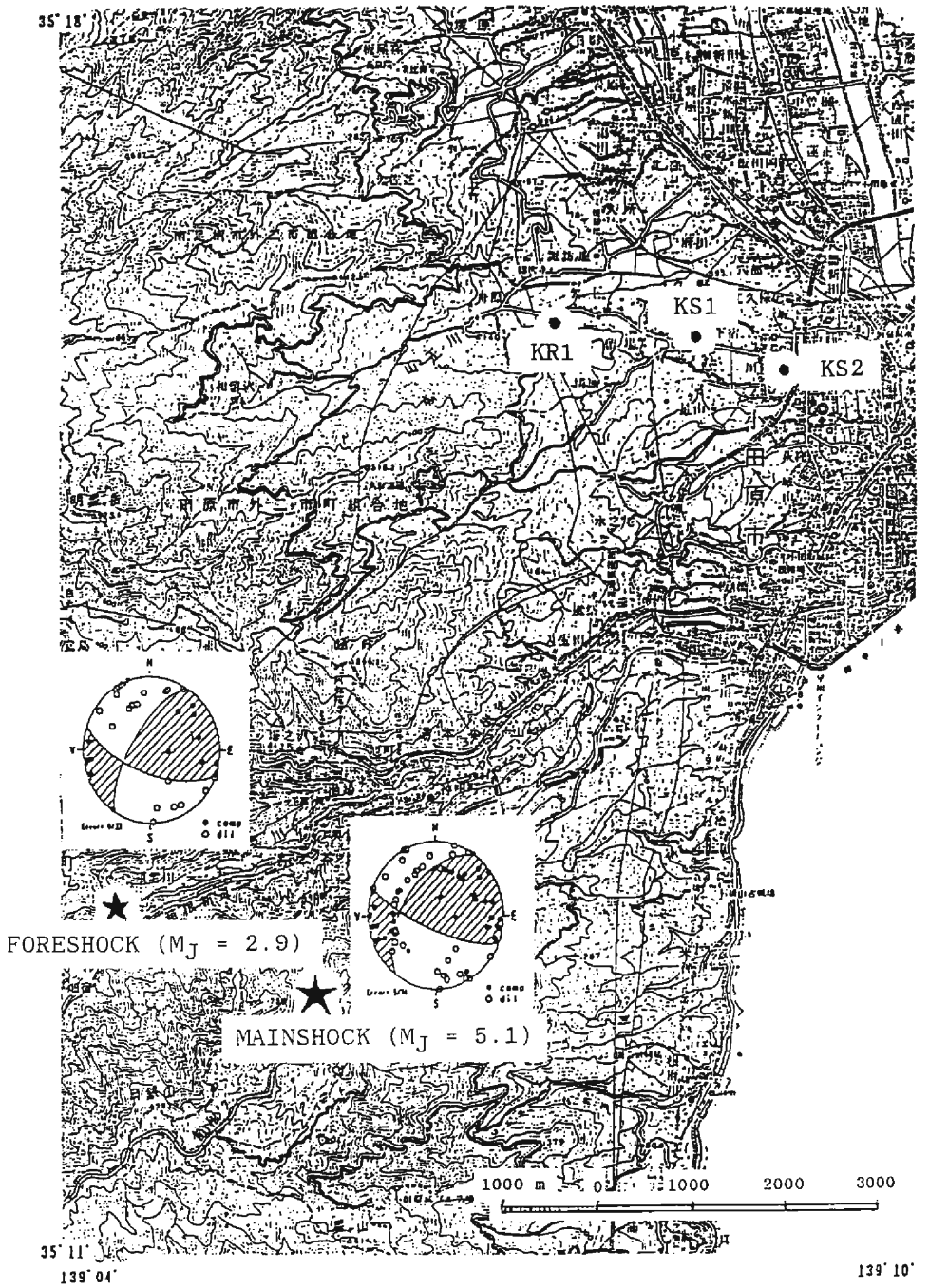

Fig. 1. Location of the epicenters of earthquakes and observation sites used in the blind prediction test. The focal mechanism solution determined by NRIESDP (1991) is also shown (after Kudo, 1992).

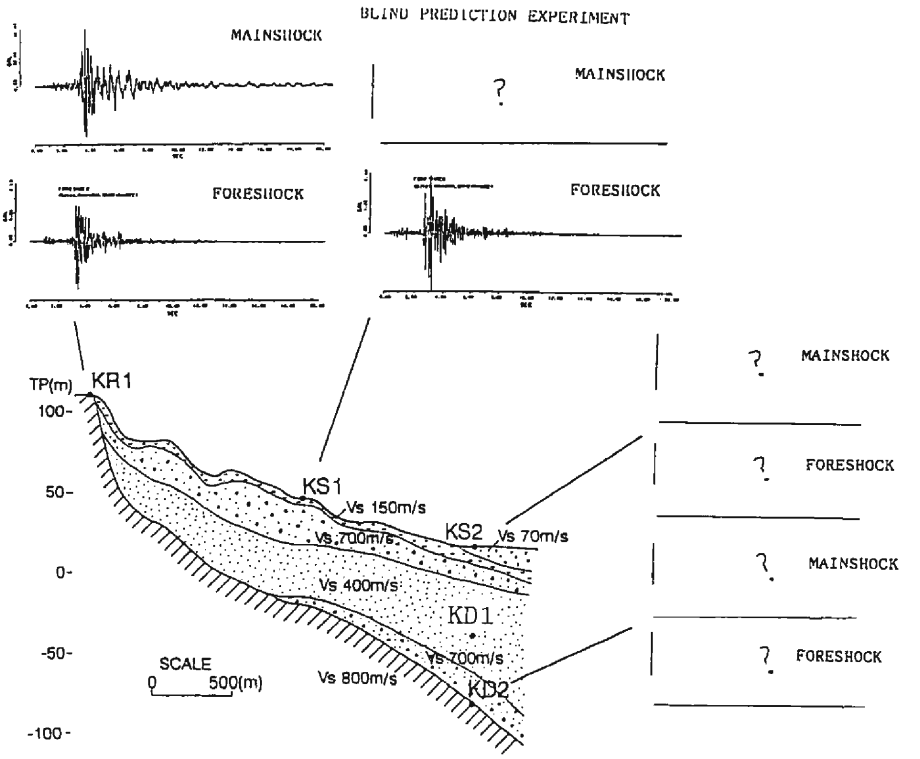

Fig. 2. Scheme of requirements for blind prediction test experiment (? means ground motion to be predicted).

predict weak and strong motions at the sediment sites given the records at the rock site (**Figure 2**). The results of the Ashigara Valley Blind Prediction Test were presented at the International Symposium on the Effects of Surface Geology on Seismic Motions held in Odawara, on March 25–27, 1992. They show a large scatter (Midorikawa, 1992) even if the same structure model is used for the numerical simulations. This confirms the extreme difficulty to model realistic underground valley structures for ground motion simulations. This study is an attempt to overcome such difficulties by using a semi-empirical approach. With this in mind, we use the empirical Green's function method combined with the scaling law of earthquakes as proposed by Irikura (1986), to simulate ground motions observed at soft soil sites of the mainshock (M=5.1). The source model for the mainshock is determined from the analysis of the mainshock and the foreshock records at rock site. This method has the great advantage of not requiring structure models (**Figure 3**). We can check the non-linear effect of soft sediments during strong motions by comparing the observed records with the simulated ones because this method is based on the linear superposition of weak motions from small events. The purposes of our paper are : 1) to compare our synthetics with the Blind prediction test results, and 2) to investigate the non-linear effect of soil by comparing the observations with the synthetics at the soft sediment sites.

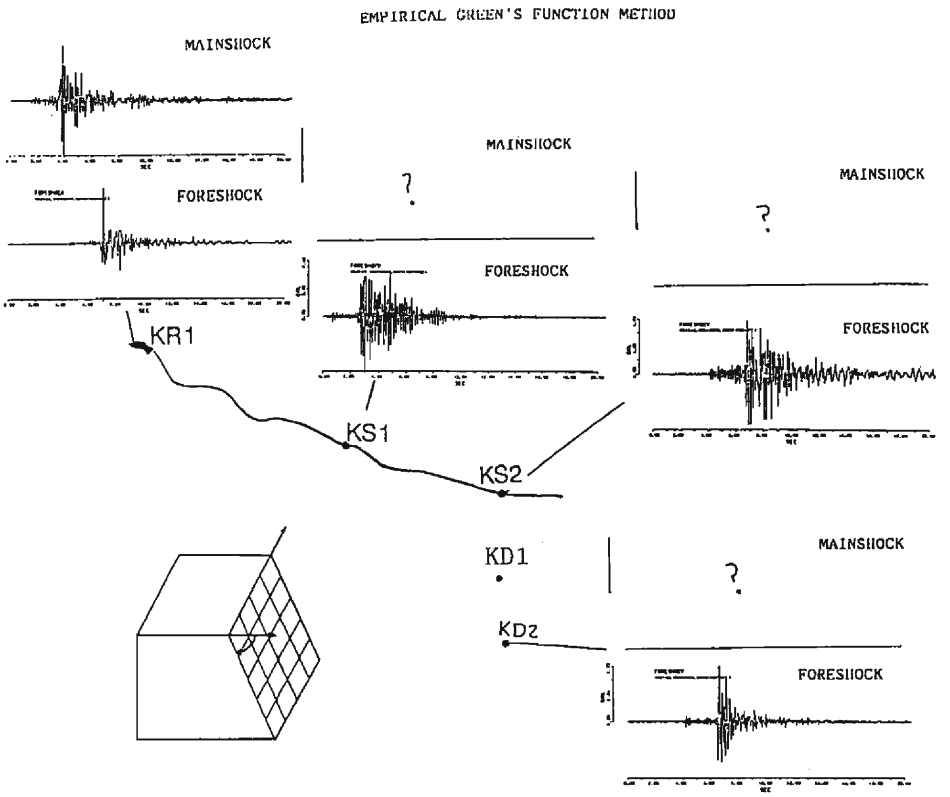

Fig. 3. Scheme of blind prediction using empirical Green's function method (? means ground motion to be predicted).

Method

The method consists essentially of a special superposition of small events. We assume that both large and small earthquakes follow the ω^{-2} spectral scaling model with a constant stress drop. Following the synthetic method for ω^{-2} model proposed by Irikura (1986), let the moment ratio between the large event to be simulated and small event used as empirical Green's function be N^3. Then, the fault area of the large event is divided into $N \times N$ subfaults. The parameter N is also obtained from the following;

$$\frac{\tilde{U}_0}{\tilde{u}_0} = \frac{M_0}{m_0} = N^3,$$
$$\frac{\tilde{A}_0}{\tilde{a}_0} = \left(\frac{M_0}{m_0}\right)^{\frac{1}{3}} = N, \tag{1}$$

where $\tilde{U}_0$, $\tilde{u}_0$ are the flat levels of the displacement spectrum (less than corner frequency), $\tilde{A}_0$, $\tilde{a}_0$ are the flat levels of acceleration spectrum (less than f_{max}) and M_0, m_0 are the seismic mo-

ments for mainshock and foreshock (or aftershock) respectively. Then, the synthetic motions $U(t)$ for the large event will be given using the small event $u(t)$ by the follow equation :

$$U(t)=\sum_{i=1}^{N}\sum_{j=1}^{N}\left(\frac{r}{r_{ij}}\right)F(t-t_{ij})*u(t), \tag{2}$$

where

$$F(t)=\delta(t)+\frac{1}{n'}\sum_{k=1}^{(N-1)n'}\delta\left[\frac{t-(k-1)\tau}{(N-1)n'}\right]. \tag{3}$$

r and r_{ij} are the distance from the hypocenter of the small earthquake and from the (i, j) element, to the site, respectively, t_{ij} is the sum of the time delay from the rupture starting point to the (i, j) element and that from the (i, j) to the site, τ is the rise time of the target event, and n' is an appropriate integer number to shift the fictitious periodicity $\tau/(N-1)$ into a high frequency out of the frequency range of interest (here $n'=80$ is used).

In order to use the record of a small event with different stress drop as empirical Green's function, we introduced a constant value C as the stress drop ratio between the large and small event :

$$C=\frac{\Delta\sigma_L}{\Delta\sigma_s}. \tag{4}$$

Since the spectral levels are affected for the same factor the equations in (1) will become :

$$\frac{\tilde{U}_0}{\tilde{u}_0}=CN'^3,$$
$$\frac{\tilde{A}_0}{\tilde{a}_0}=CN', \tag{5}$$

and the equation (2) will be modified replacing $u(t)$ with $Cu(t)$ and N with N' as follows :

$$U(t)=\sum_{i=1}^{N'}\sum_{j=1}^{N'}\left(\frac{r}{r_{ij}}\right)F(t-t_{ij})*Cu(t). \tag{6}$$

More details about the parameter C are shown in the Appendix.

Data

The strong motion records were obtained from the $M_{JMA}=5.1$ earthquake that occurred on August 5, 1990, in the west part of Kanagawa Prefecture, called the 1990 Hakone earthquake. The other event is the biggest foreshock $M_{JMA}=2.9$, which occurred approximately two hours before the mainshock. Based on the focal mechanism determined by NRIESDP (1991) for the mainshock, we adopted the plane B(strike=N106°E, dip=72°) as the fault plane. The aftershock distribution $3.0\times3.0\text{km}^2$(also reported by NRIESDP (1991)) was assumed to be the source area.

Ground acceleration was recorded at the five sites KR1, KS1, KS2, KD1 and KD2

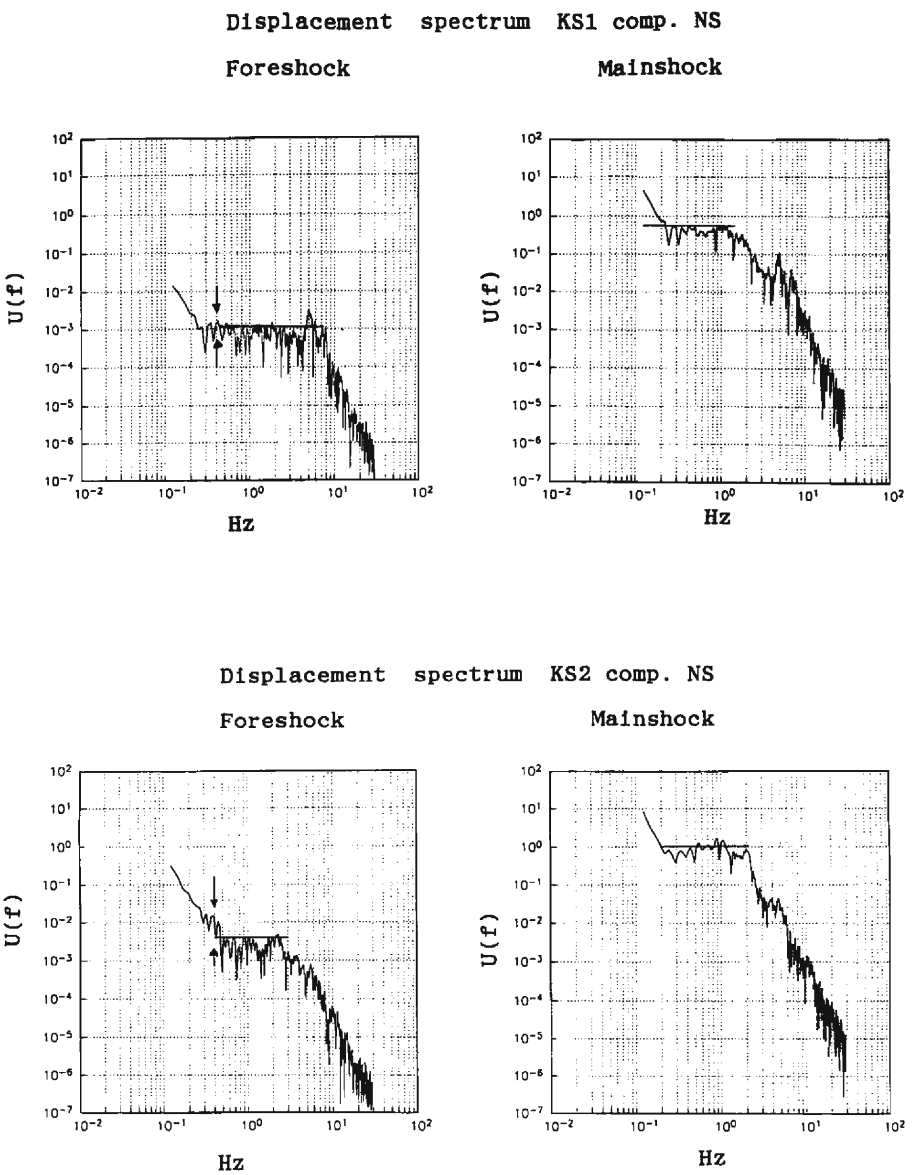

Fig. 4. Displacement spectra for foreshock (left) and mainshock (right), at sites KS1, KS2, KD1, and KD2.

(**Figure 2**). Based on the analysis of the acceleration and displacement amplitude spectra at the five sites, the reliable frequency range was found to be from 0.4 Hz to 10 Hz for KR1, KS1 and KS2; and from 0.9 Hz to 10 Hz for KD1 and KD2, due to the low signal levels for the small event compared with the noise levels which are least at the borehole sites (**Figure 4**).

We obtained the low frequency flat levels of displacement spectra and the high frequency

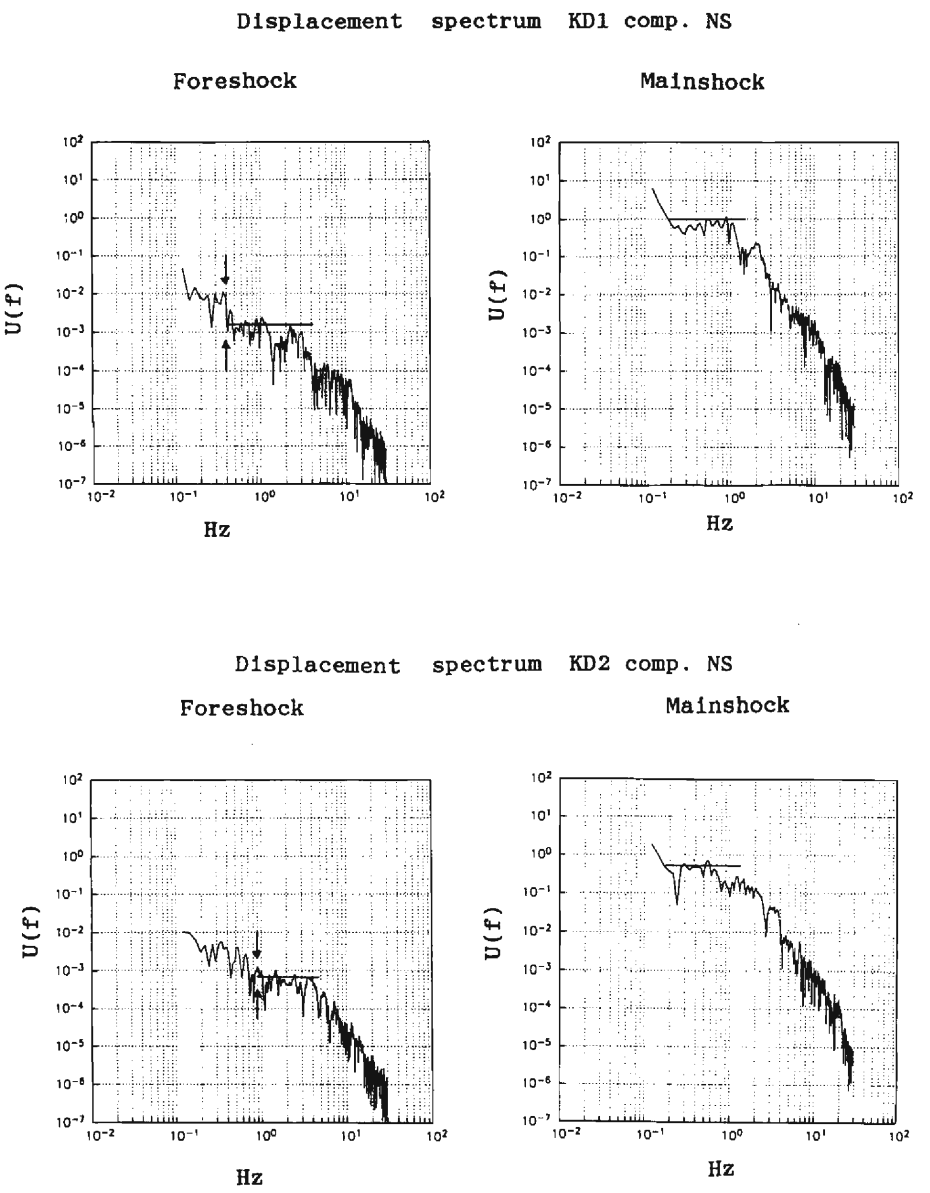

Fig. 4. (Continued)

flat levels of acceleration spectra at the rock site, KR1, for both events, as shown by straight lines in the upper and lower panels of **Figure 5**. The spectral ratio of the NS component at KR1 is shown together with low and high frequency ratio levels in the middle of **Figure 5**. The ratio levels (low frequency : 680, high frequency : 40) depart largely from the relation given in equation (1) for the ω^{-2} model. This comes from the difference in stress drop be-

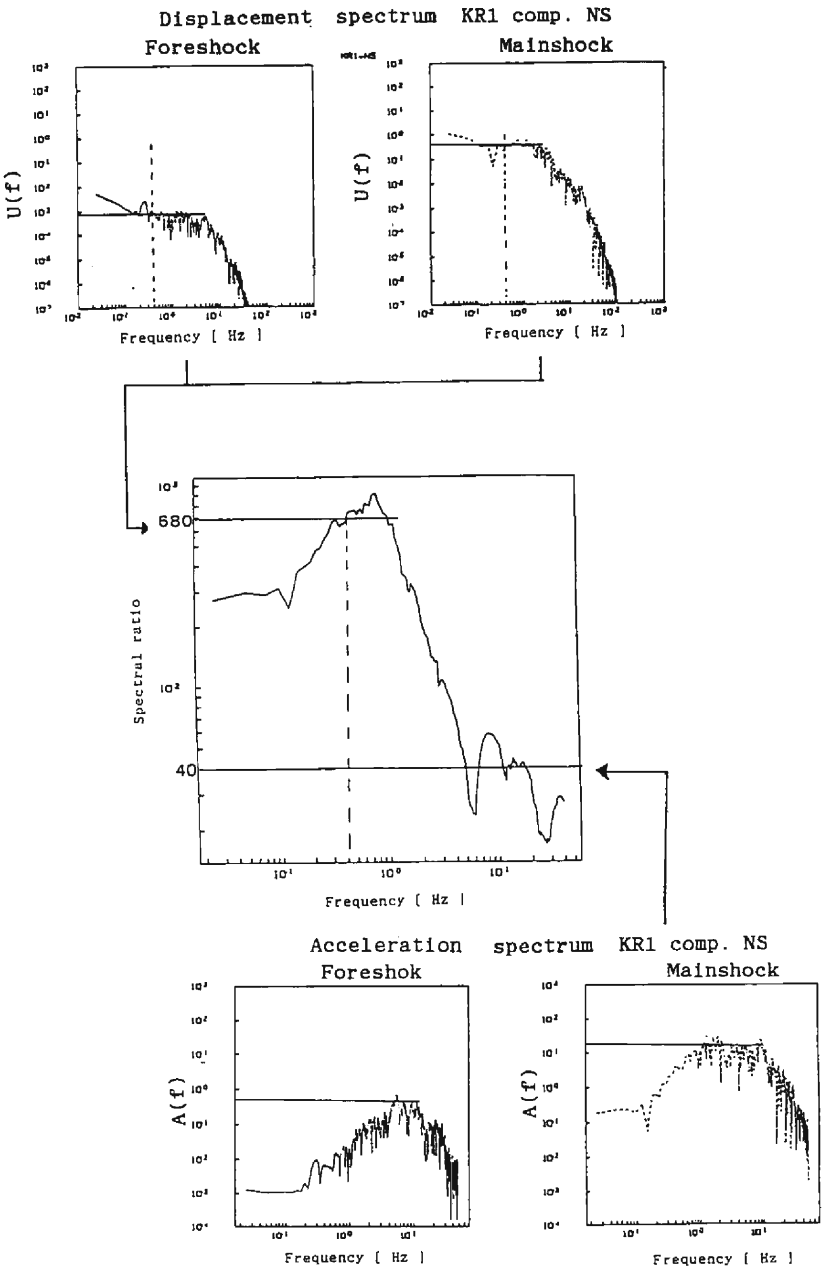

Fig. 5. Spectral ratio between mainshock and foreshock at KR1, station, component NS.

tween the two events.

Model

For the initial source model of the target event, we assumed a source dimension of 3.0× 3.0km^2(based on the aftershock distribution) with the strike direction of N106^{0}E and dip angle of 72^0(NRIESDP, 1991). The rupture is propagated radially from the starting point (to be defined) at constant velocity V_r=2.35 as 0.72V_s(V_s : S wave velocity), and the rise time, 0.16 seconds. That model is shown schematically in **Figure 6**. Since the stress drop of the target event is different from the small event we have to apply an appropriate method, i. e. the modified equations (4) to (6). Then, we obtain the synthetic parameters N =4 and C=9.7 based on the ratio levels following the procedure shown in the Appendix. We needed to assume more parameters to simulate ground motion from the source model such as rupture velocity, rise time, and rupture starting point in the source area. We found them by forward modeling. We found that synthetics were insensitive to variations of the rupture velocity and the rise time, but very sensitive to the location of the rupture starting point. The best starting point was determined to be close to the center bottom of the fault plane (see **Figure 6**). Next,

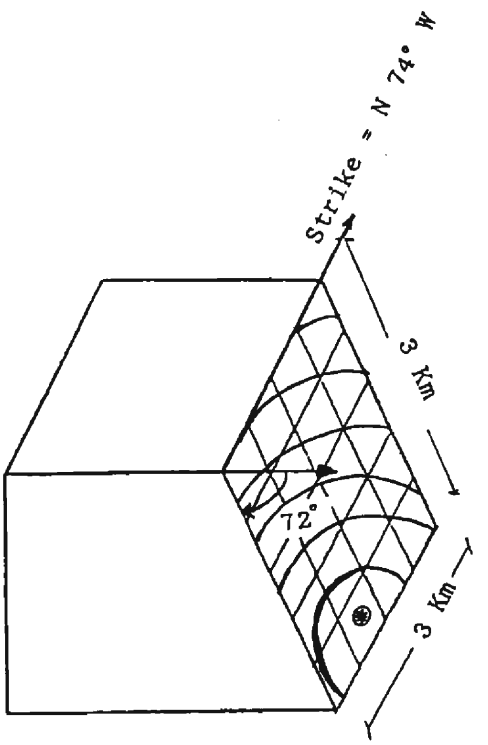

Fig. 6. Source model used.

we determined the best model minimizing the residual between the observed and the synthetic waveforms within a time window including the main motions, changing only the value C. Two cases are studied here. One is when all of a waveform is taken into consideration; the other one is a 3 second comparison window, restricted just to the main part of the movement (upper left waveforms of **Figures 7–11**). The smallest residual value was reached with C equal to 6.5 and 8.0 for the first and second cases, respectively. The above procedure was applied to fit the observed records simultaneously at KR1 and KD2. In each case, the components were weighted, based on the peak to peak amplitude of the observed waveform.

Results

First let us discuss the source model considered in the first case ($C=6.5$). After the model was completely defined, we used it to compute the synthetic motions at the other sites, at KS1, KS2 and KD1. These simulations are shown in **Figures 7** to **11**, where we can see the velocity and acceleration simulations with the respective observed waveforms. For all the sites, the fitting between the observed and synthetic one is very good from the S wave's onset through the coda part in velocity waveforms of NS component and good in the main part of the EW component. The signal–noise ratio is relatively small for the EW component records of the small event, specially low at the borehole sites, KD1 and KD2. This is the reason why the simulations are relatively not good in the EW component. It is also comprehensible why the EW component synthetic motions at KD1 and KD2 appear to be strange (**Figures 10** and **11**). For the KS1 site, the synthetic velocity waveform is very similar to that observed not only in the NS but also EW components. However, for the EW component, the peak value of the synthetic appears to be overestimated a little, compared with that of the observed one (**Figure 8**). The velocity simulation of NS component at KS2 agrees well with the observed one, but the simulation of EW component does not. This is probably because the signals are contaminated by background noises. Even so, the main part of the synthetic velocity of the EW component is consistent with the observation. On the other hand, the agreement between synthetic accelerations and the observed ones at KS2 and KD1 is better than that of velocity waveforms (**Figures 9** and **10**), although, like in the case of velocity, the NS acceleration component still is better than the EW acceleration component. For the rest of the sites, peak accelerations of the simulations are in good agreement with those of the observed records. Only at KS1 site, did we find the synthetic peak accelerations of both components (NS and EW) to be a little overestimated. This overestimation does not appear at KS2.

Now let us consider the second case when we focused on the main movement and $C=8.0$. This time the main part of acceleration movement was synthesized using a 3-second window. The simulations and observed waveforms are shown in **Figures 13** and **14**. By a very simple inspection a difference in amplitude between the observed and synthetic acceleration waveforms can be seen, which is related to the two soft soil sites KS1 and KS2. We compared the peak to peak amplitudes in order to be objective in the evaluation of those differences. The peak to peak amplitude rationalized with respect to the observed amplitude is shown in **Figure 15**. In this graphic is easier to see the difference between simulations at KD1, KD2, and KR1

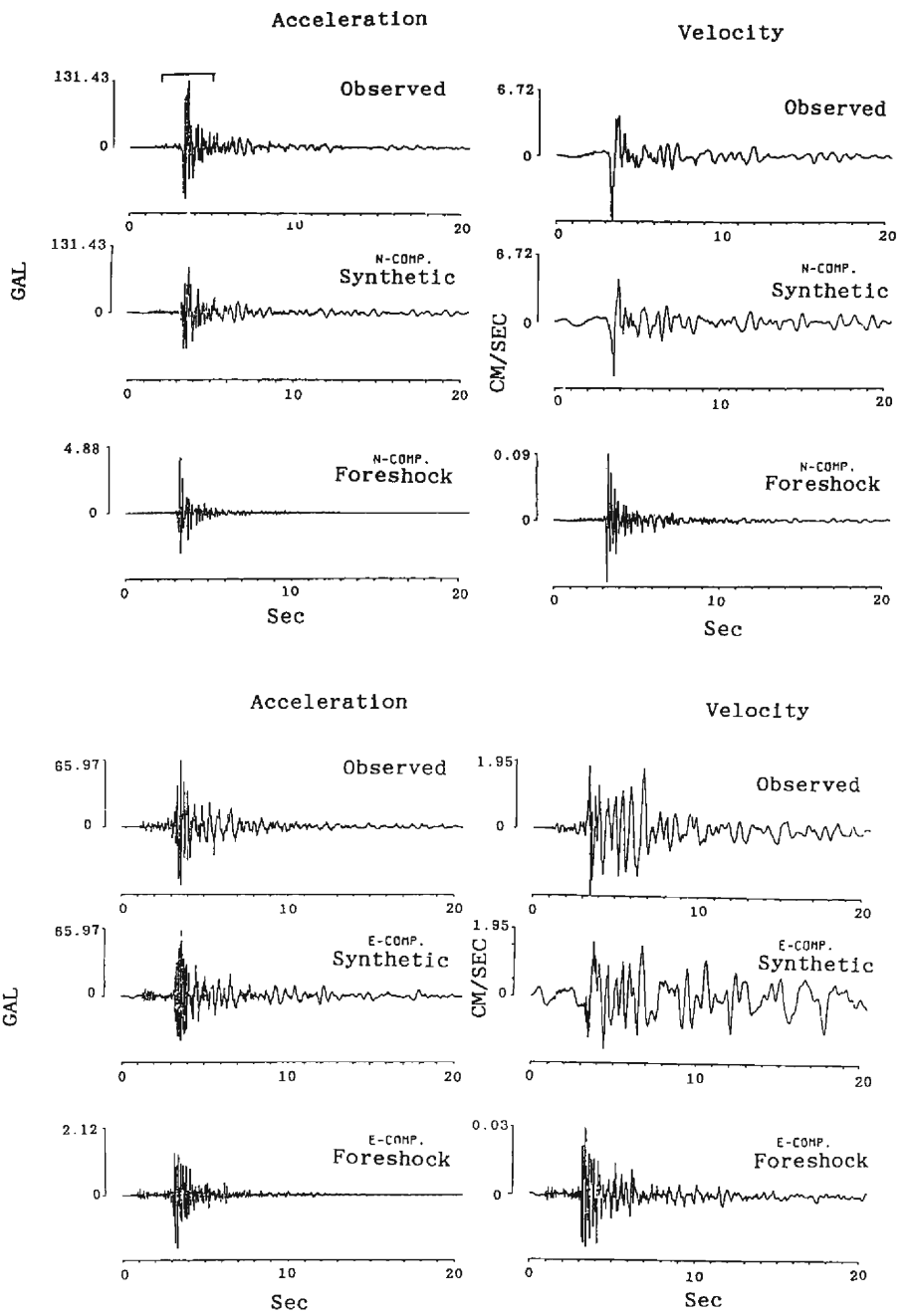

Fig. 7. Simulation at KR1 site. Upper : NS component, Lower : EW component. Left : Acceleration, Right : Velocity. From top to bottom : observed, synthetic and foreshock. (Note the different scale for the foreshock record).

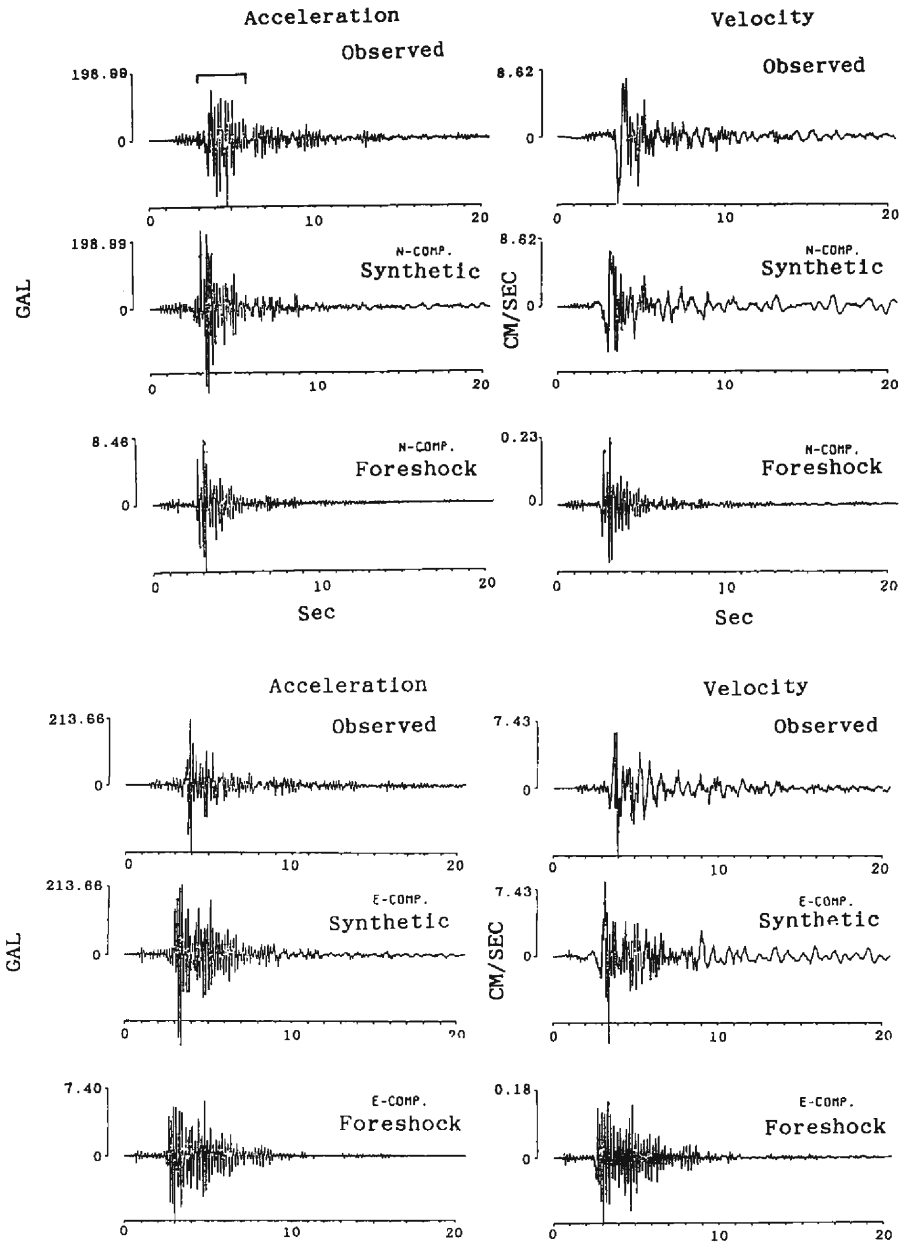

Fig. 8. Simulation at KS1 site. Upper : NS component, Lower : EW component. Left : Acceleration, Right : Velocity. From top to bottom : observed, synthetic and foreshock. (Note the different scale for the foreshock record).

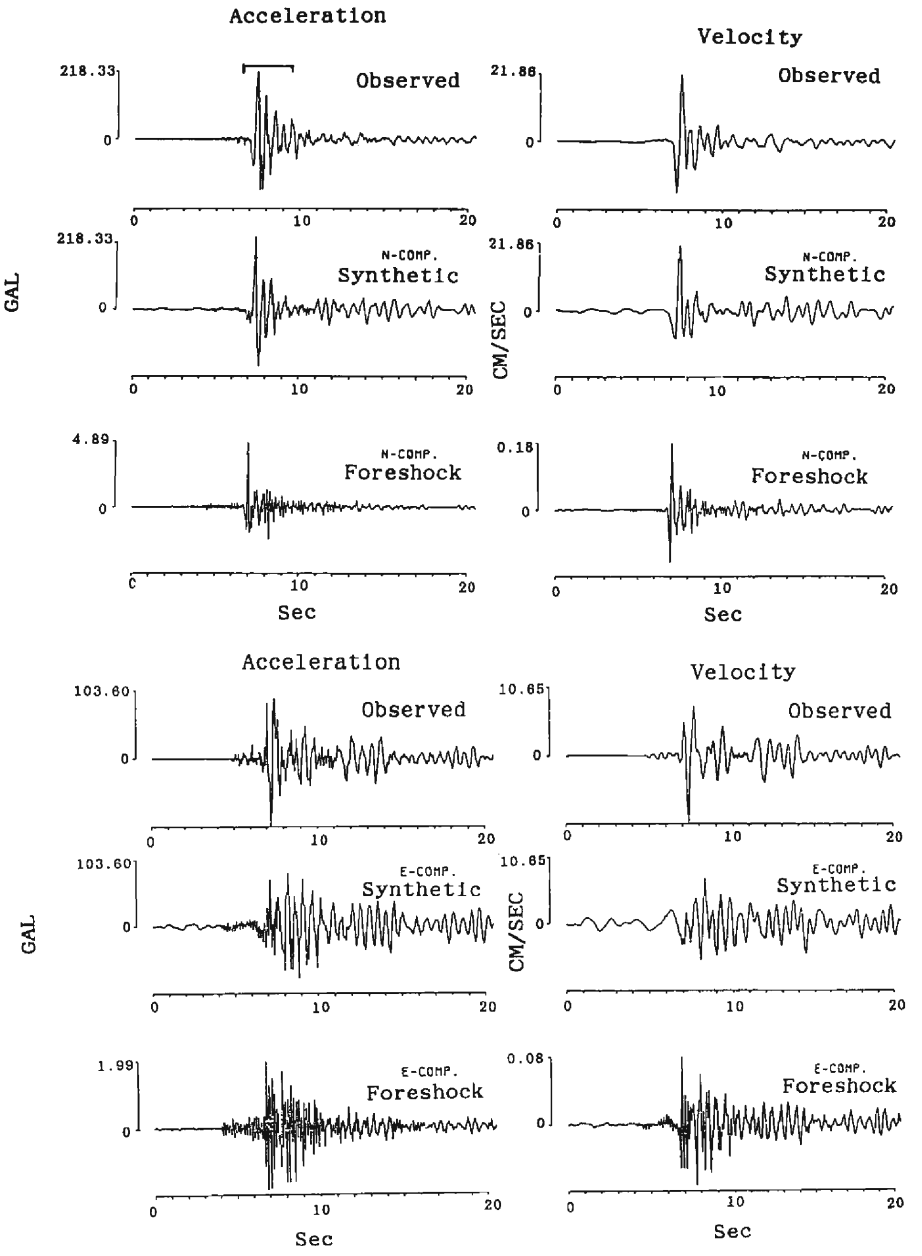

Fig. 9. Simulation at KS2 site. Upper : NS component, Lower : EW component. Left : Acceleration, Right : Velocity. From top to bottom : observed, synthetic and foreshock. (Note the different scale for the foreshock record).

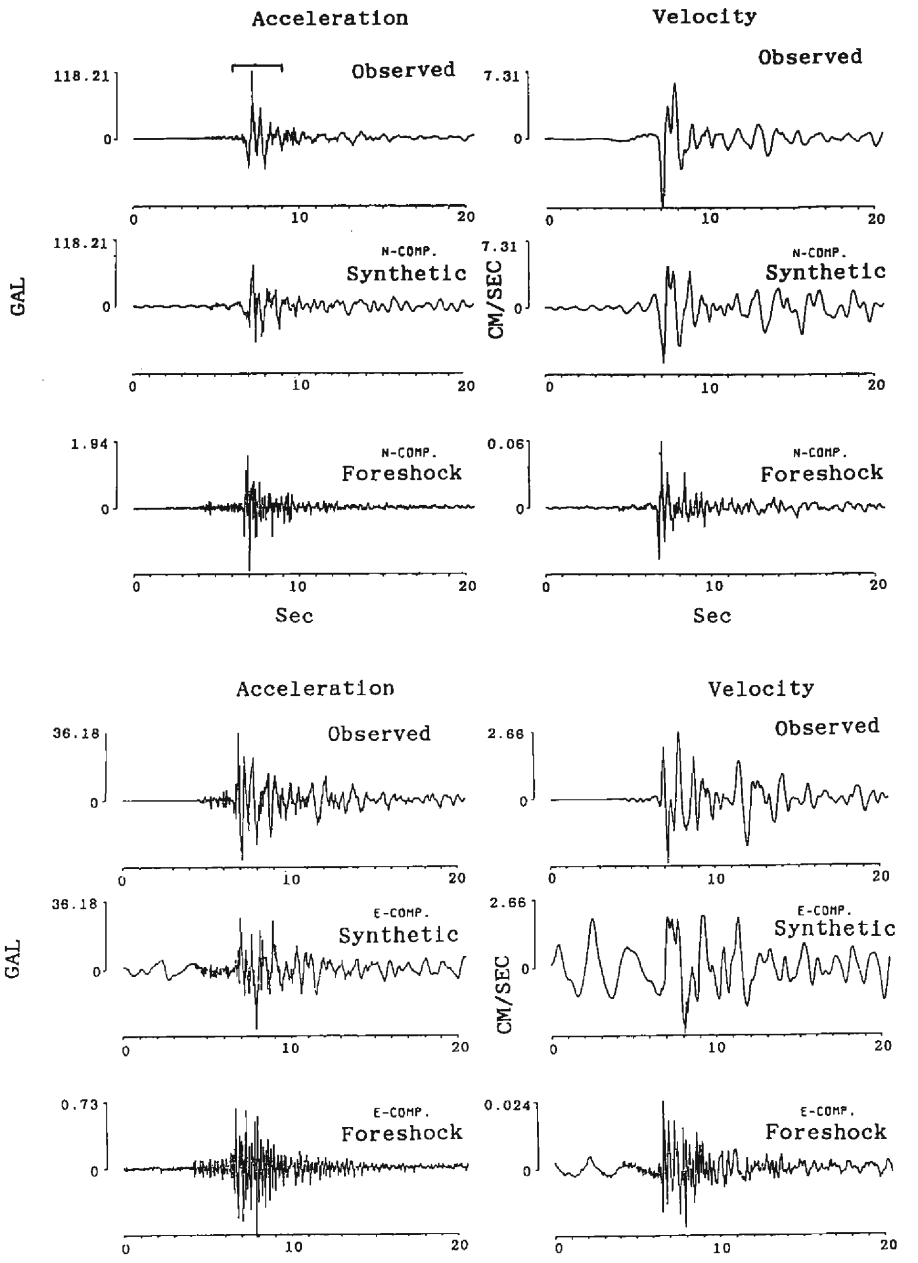

Fig. 10. Simulation at KD1 site. Upper : NS component, Lower : EW component. Left : Acceleration, Right : Velocity. From top to bottom : observed, synthetic and foreshock. (Note the different scale for the foreshock record).

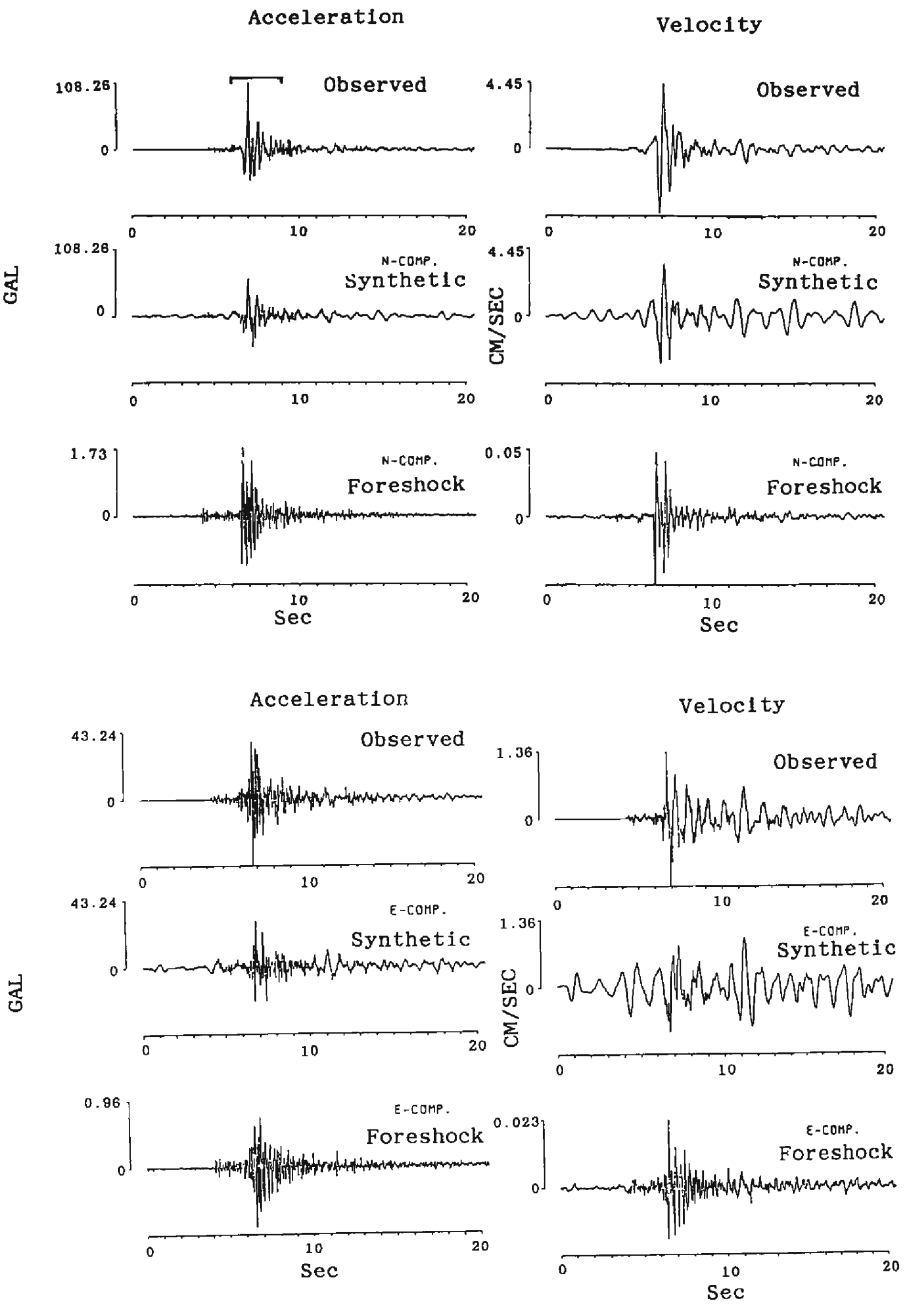

Fig. 11. Simulation at KD2 site. Upper : NS component, Lower : EW component. Left : Acceleration, Right : Velocity. From top to bottom : observed, synthetic and foreshock. (Note the different scale for the foreshock record).

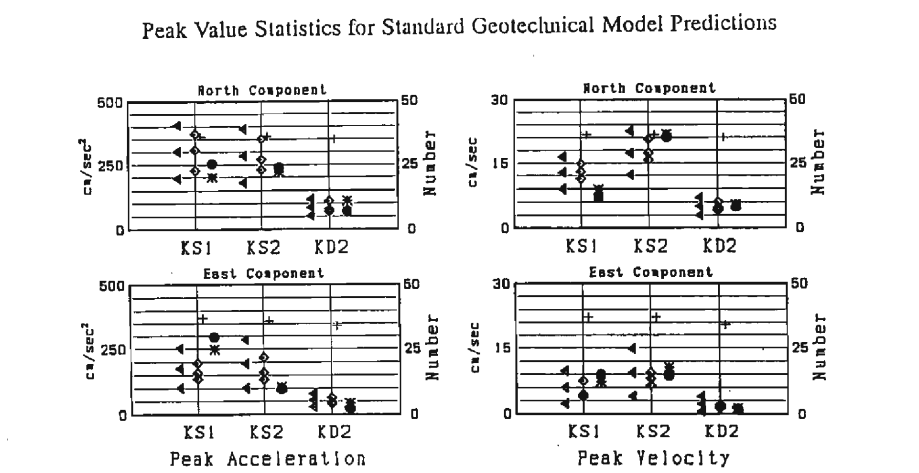

Fig. 12. Peak value statistics for standard Geotechnical model predictions from blind prediction experiment (after Midorikawa, 1992), and the peak values obtained from this paper.

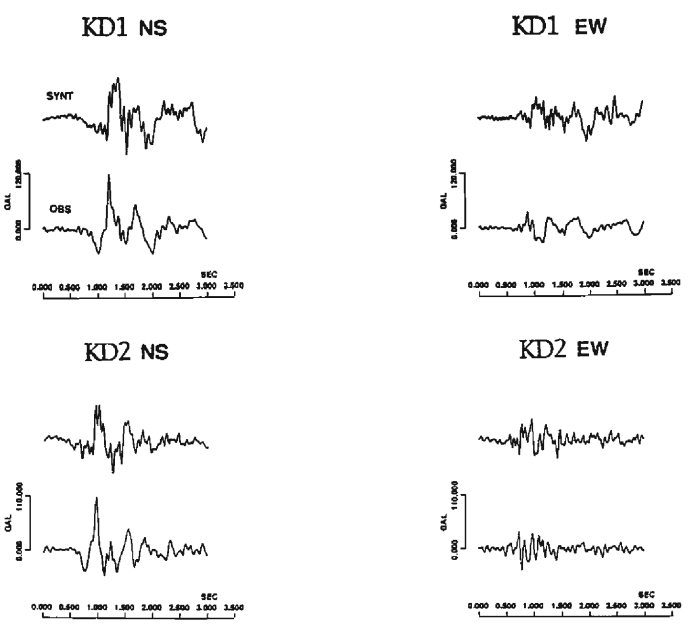

Fig. 13. Acceleration waveforms, synthetic (above) and observed (below), at KR1, KS1 and KS2. Left : component NS, right : component EW. Synthetics are calculated with (C=8.0).

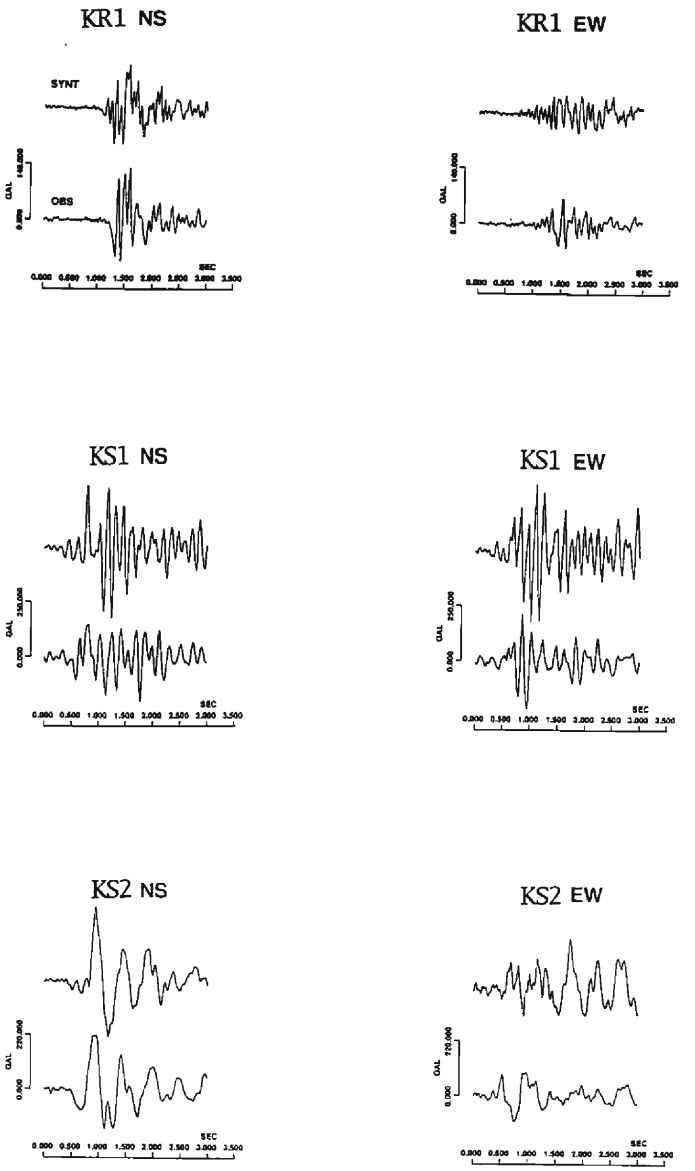

Fig. 14. Acceleration waveforms, synthetic (above) and observed (below), at KD1 and KD2. Left : component NS, right : component EW. Synthetics are calculated with (C=8.0).

with respect to that of KS1 and KS2. Note that in this case the error is small enough to be differentiable of non linear effect. In **Figures 16** and **17** the comparison between peak to peak velocities is shown. In this case the results became uncertain because the non-linear effect is comparable in dimension with the error **(Figure 18)**. Another possible interpretation is that

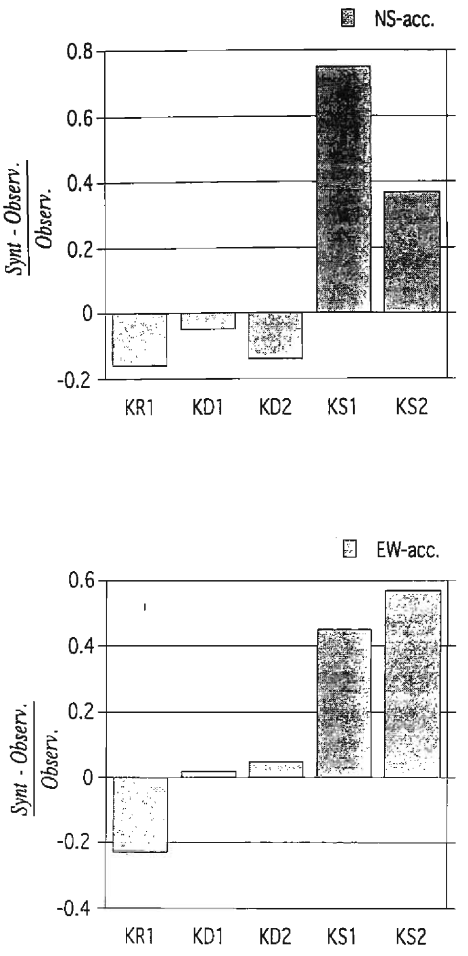

Fig. 15. Differences in peak to peak values between the synthetic and observed accelerations.

the non–linear effect operates at high frequency, since the apparent frequency for peak acceleration (for example at KS2–NS, 1.8 Hz) is different from the apparent frequency for peak velocity (for KS2–NS 1.3 Hz), and so does not appear in velocity records. Also from the comparison of the acceleration and velocity spectra, we could not find systematic changes of the predominant frequencies between the observed and synthetic at KS1 and KS2 (**Figure 19**).

Discussion

In general, the results obtained here show better agreement than most of the predictions submitted to the Ashigara Blind Prediction Test at Odawara Symposium (Midorikawa, 1991).

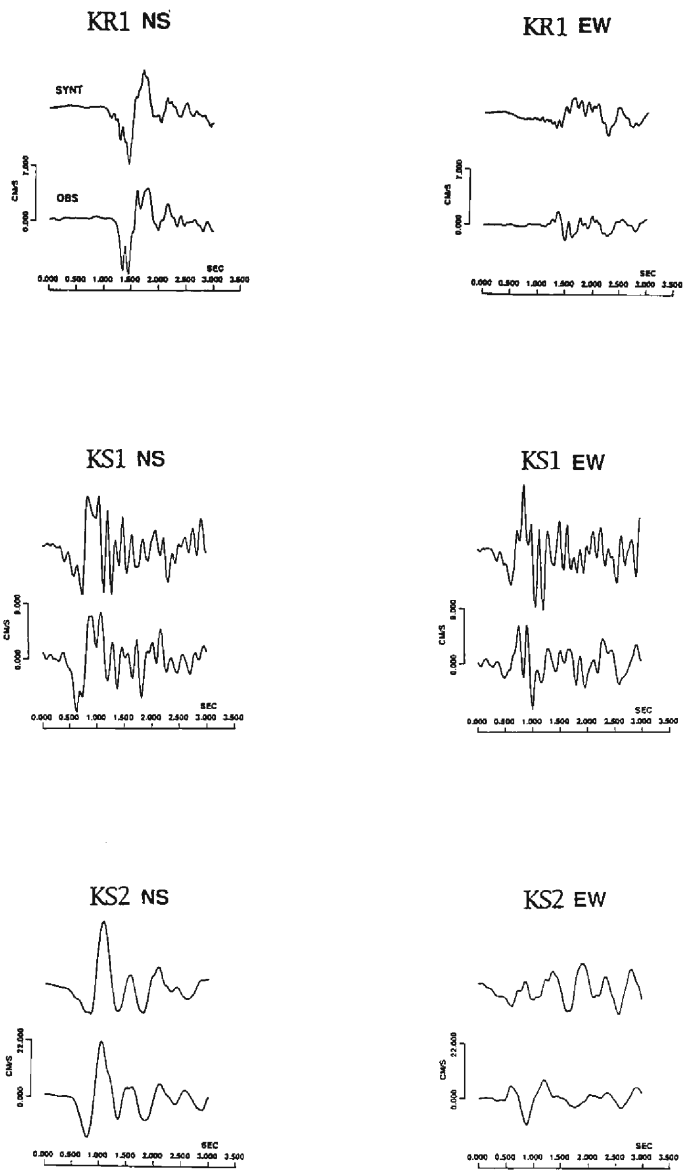

Fig. 16. Velocity waveforms, synthetic (above) and observed (below), at KR1, KS1 and KS2. Left : component NS, right : component EW. Synthetics are calculated with (C=8.0).

The peak amplitudes for our predicted acceleration and velocity are shown together with those of the predictions submitted to Ashigara Experiment in **Figure 12.**

To discuss the non-linear effect, which is the main purpose of this paper, we should consider the strong and week points of the procedure that we followed. The Empirical Green's

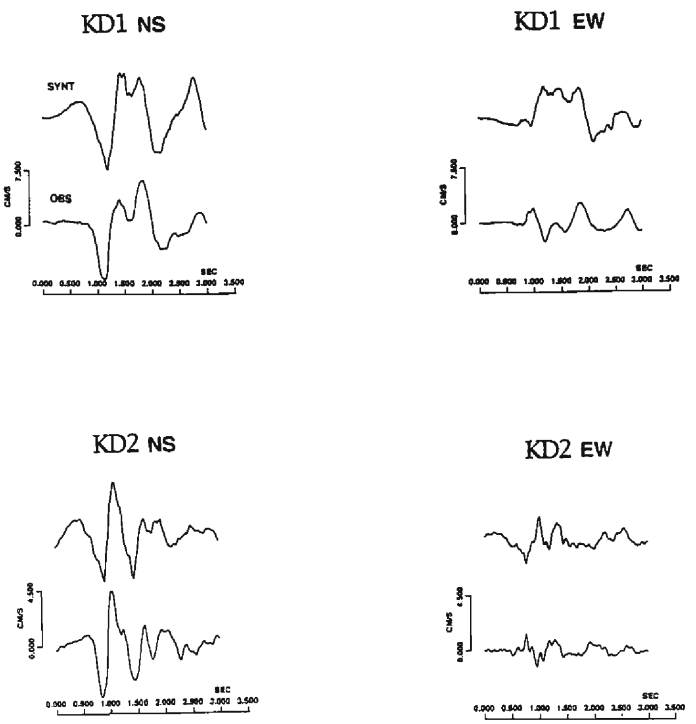

Fig. 17. Velocity waveforms, synthetic (above) and observed (below), at KD1 and KD2. Left : component NS, right : component EW. Synthetics are calculated with (C=8.0).

Function Method considers the linear behavior of the medium. It can produce a good simulation if the source model could be accurately simulated. Here we consider the simple model with constant rupture velocity, constant displacement and constant stress drop along the whole fault area. Therefore, the simulations have an amount of error due basically to the simplification of the source model. However, it still can discuss the differences that surpass such amounts of error. In this case another factor arises, a correction for the differing stress drop between the small and large earthquake was carried out and constituted a very important factor for the final results, so that special attention was given to the determination of that correction. We can discuss relative variations of strong motion estimation between hard rock and soft soil sites, even if the absolute values of differences are not so reliable. The short time window gives better agreement between observation and calculations at the underground sites KD1 as well as KR1. This means that longer time window data for the small event have contamination due to background noise because of low S/N ratios. Two different values of C were found depending on the time duration of the comparison window used to minimize the error. For the simulation with $C=6.5$, only small differences between observation and simulation were found at KS1, while the simulation with $C=8.0$ showed clear overestimation at KS1 and KS2 sites. We interpret these results as indicating that a non-linear effect of soil restricted to a very limited portion of the strong motion exists. This is in agreement with

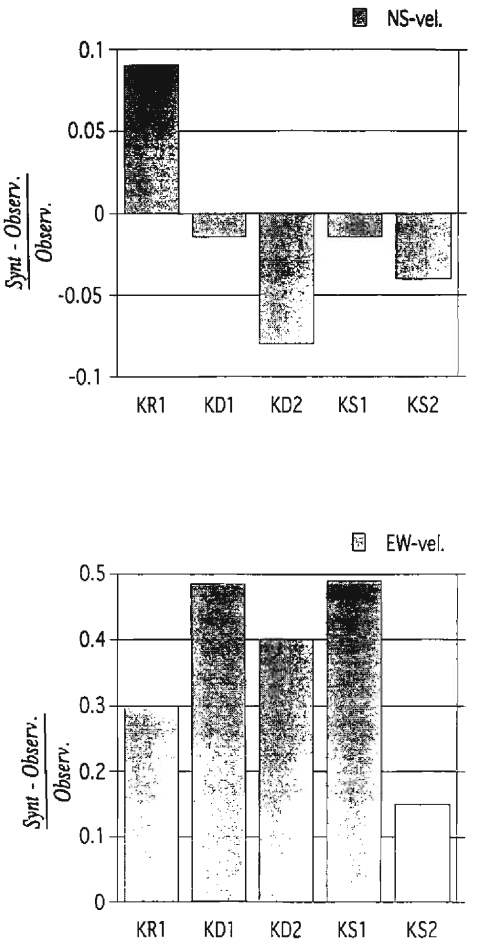

Fig. 18. Differences in peak to peak values between the synthetic and observed velocities.

Satoh et al. (1992) results.

Conclusion

We simulated ground motions at a site on a rock outcrop (KR1), at two soft soil sites (KS1 and KS2), and at two borehole sites in sediments (KD1 and KD2) from the 1990 Hakone earthquake ($M_{JMA}=5.1$) using the records of the foreshock with $M_{JMA}=2.9$ as the empirical Green's function.

We found that the stress parameter of the foreshock was different from that of the mainshock based on the spectral ratio between both events at the rock site KR1. Then, the simula-

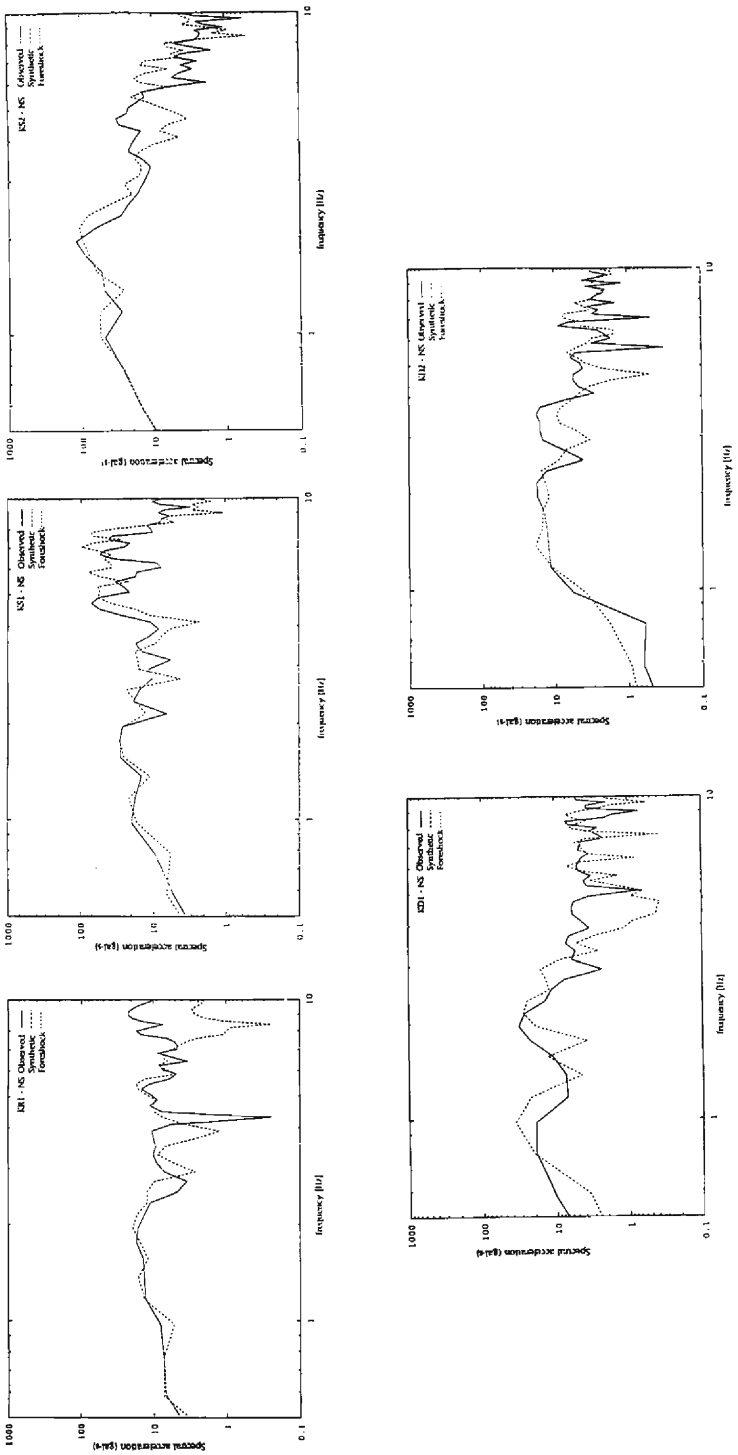

Fig. 19. Fourier spectra of synthetic and observed accelerations at KR1, KS1, KS2, KD1 and KD2 sites.

tion method for the ω^{-2} model proposed by Irikura (1986) was revised in order to be applicable to the case when a small event with different stress parameter from that of the mainshock is used.

We could not find any clear differences between the observed and synthetic using the best model determined from a wide window (30 seconds). Using a 3–second window, the differences among the accelerations of synthetics and observed are clearly greater at KS1 and KS2 than at the rest of the sites.

From the comparison of their spectra, we could not find systematic changes of the predominant frequencies between the observed and synthetic at KS1 and KS2.

We conclude that non–linear effect during the 1990 Hakone earthquake ($M_{JMA}=5.1$) exists at KS2 and KS1, based on the overestimation of peak simulated accelerations obtained by a linear simulation of the observed ones.

Acknowledgment

The Ashigara Blind Prediction Test held in March 1991 has been organized by the Japan ESG Working Group cooperatively with the IASPEI/IAEE Joint Working Group on ESG (Chairmans R. O. Iwan and B. Turcher). We sincerely thank K. Kubo and other key members of the Japan ESG W. G. for their work devoted to the Project. We also thank K. Hirahara and an anonymous reviewer for their reviews of the manuscript.

References

Brune, J. N. (1970), Tectonic stress and the spectra of seismic shear waves from earthquakes, J. Geophys. Res., 76, 4997–5002.

Irikura, K. (1986), Prediction of strong acceleration motions using empirical Green's function, Proc. 7th Japan Earthq. Eng. Symp., 151–156.

Kudo, K. (1992). Earthquake motions : Given and Blinded Data, Proceedings of International Symposium on the Effects of Surface Geology on Seismic Motion, Vol. II, 53–60.

Midorikawa, S. (1992). A statistical analysis of the submitted predictions for Ashigara Valley Blind Prediction Test, Proceedings of International Symposium on the Effects of Surface Geology on Seismic Motion, Vol. II, 65–77.

National Research Institute for Earth Science and Disaster Prevention (1991), The Earthquake in the Western Part of Kanagawa Prefecture (August 5, 1990), Report of the coordinating Committee for Earthquake Prediction, Vol. 45, 213–220.

Satoh, T., Sato, T. and Kawase, H. (1992), Local site effects on weak and strong motions at the Ashigara Valley, Japan, Presented at International Sym. on Earthquake Disaster Prevention (May 1992, Mexico city).

Appendix

Estimation of stress parameter.
Stress parameter, $\Delta\sigma$, is given as

$$\Delta\sigma = k\, M_0 fc^3, \tag{A-1}$$

where

M_0 : seismic moment
fc : corner frequency
$k=(1/0.49\beta)^3$ for circular crack (Brune, 1970)

For ω^2 model, flat level of acceleration spectra, a_0, is given as

$$a_0 = fc^2 M_0 \tag{A-2}$$

$$fc = (a_0/M_0)^{0.5} \tag{A-3}$$

From (A-1) and (A-3), stress parameter is given as

$$\Delta\sigma = k\, M_0 (a_0/M_0)^{1.5} = k\, M_0^{-0.5}\, a_0^{1.5} \tag{A-4}$$

Estimation of seismic moment, M_0, and source acceleration spectral amplitude, a_0.

The spectral level of displacement at low frequencies, $u_{l.f.}$, and that of a acceleration at high frequencies ($<f_{max}$), $a_{h.f.}$ are given as

$$\tilde{u}_{l.f.}(r, \theta, \varphi) = \frac{R_{\theta\varphi}}{4\pi r\rho\beta^3} M_0 \exp[-\pi fr/\beta Q(f)] \tag{A-5}$$

$$\tilde{a}_{h.f.}(r, \theta, \varphi) = \frac{R_{\theta\varphi}}{4\pi r\rho\beta^3} a_0 \exp[-\pi fr/\beta Q(f)] \tag{A-6}$$

Therefore, M_0 and a_0 at (A-4) are estimated from (A-5) and (A-6). The ratio of stress drop between large and small events, i. e. factor C, is expressed as follows, from (A-1), (A-4), (A-5), and (A-6).

$$c = \frac{\Delta\sigma^L}{\Delta\sigma^S} = \left(\frac{\tilde{u}^L_{l.f.}}{\tilde{u}^S_{l.f.}}\right)^{-\frac{1}{2}} \left(\frac{\tilde{a}^L_{h.f.}}{\tilde{a}^S_{h.f.}}\right)^{\frac{3}{2}} \tag{A-7}$$

That is, to obtain C, we need to know only the spectral ratio at low frequencies and the spectral ratio at high frequencies between large and small events. Probably, the above estimation is more stable than Brune's method (1970) using M_0 and f_C.